

Topological Mott Insulator at Quarter Filling in the Interacting Haldane Model

Peizhi Mai¹, Ben Feldman^{2,3,4}, and Philip W. Phillips^{1,*}

¹Department of Physics and Institute of Condensed Matter Theory, University of Illinois at Urbana-Champaign, Urbana, IL 61801, USA

²Geballe Laboratory of Advanced Materials, Stanford, CA 94305, USA

³Department of Physics, Stanford University, Stanford, CA 94305, USA

⁴Stanford Institute for Materials and Energy Sciences, SLAC National Accelerator Laboratory, Menlo Park, CA 94025, USA

While the recent advances in topology have led to a classification scheme for electronic bands described by the standard theory of metals, a similar scheme has not emerged for strongly correlated systems such as Mott insulators in which a partially filled band carries no current. By including interactions in the topologically non-trivial Haldane model, we show that a quarter-filled state emerges with a non-zero Chern number provided the interactions are sufficiently large. We establish this result first analytically by solving exactly a model in which interactions are local in momentum space. The exact same results obtain also for the Hubbard interaction, lending credence to the claim that both interactions lie in the same universality class. From the simulations with determinantal quantum Monte Carlo, we find that the spin structure at quarter filling is ferromagnetic for the topologically non-trivial case. Possible experimental realizations in cold-atom and solid state systems are discussed.

1 Introduction

To a large extent, topology and strong electron correlation, the two pillars of quantum materials, have evolved essentially independently. The highly successful classification scheme^{1,2} of band insulators into topologically trivial or non-trivial assumes the electrons are non-interacting and hence only the details of the band structure are relevant. In the other extreme lies the physics of doped Mott insulators, the parent state of copper-oxide high-temperature superconductors. As Mott insulation traditionally obtains

in a half-filled band, it naturally implies a breakdown of the single-particle concept. Further, Mott insulation is generally formulated in real-space from on-site interactions and topological invariants require a momentum-space picture. How is it then possible to formulate a topological classification scheme for Mott insulators?

In this paper we show how this is possible and the operative mechanism suggests that a momentum-space formulation of Mott insulation is more telling than the standard real-space formulation. We prove that the interacting quarter-filled band in the Haldane model¹ is a topologically non-trivial Mott insulating state should the interactions exceed the bandwidth. The ground state is ferromagnetic and has the appropriate topological feature associated with the lifting of the spin degeneracy, namely an odd Chern index. We establish this result in two ways. We first demonstrate this exactly from an interacting model^{3,4} and then we solve the Hubbard version of this model using determinantal quantum Monte Carlo (DQMC). It is from the DQMC results that we are able to resolve the ferromagnetic nature of the insulating ground state. Aside from establishing for the first time the existence of a topological Mott insulator, the consilience between the exactly solvable model and the Hubbard results further amplifies our previous demonstration⁵ that a fixed point that breaks Z_2 symmetry controls Mott physics.

To uncloak topological features of Mott physics, we note that although traditionally topology is concerned with the equivalent ways of distorting a geometric object, it is the algebraic formulation that is most relevant to condensed matter systems. Consider the energy spectrum of some quantum mechanical system. Any continuous deformation of the underlying Hamiltonian, keeping the same boundary conditions, which leaves the bulk physics unchanged is inherently topological. It is this realization^{1,2} that accounts for the stability of edge currents in the quantum Hall⁶ effect and protects the surface states^{2,7-12} in topological insulators from acquiring a gap. While it is a large perpendicular magnetic field that creates the edge currents in quantum Hall systems, the same physics obtains even in the absence of a net magnetic field. In practise, topological insulation arises either from the relativistic effect resulting from the a spin-dependent force or spin-orbit coupling^{2,7-12} or complex hoppings on a honeycomb¹ as in Fig. 1 or square lattices¹⁰ with net zero but inhomogeneous magnetic fields. The hallmark of bands with non-trivial topology is a non-zero Chern number¹³ which is computable entirely from the single-particle states.

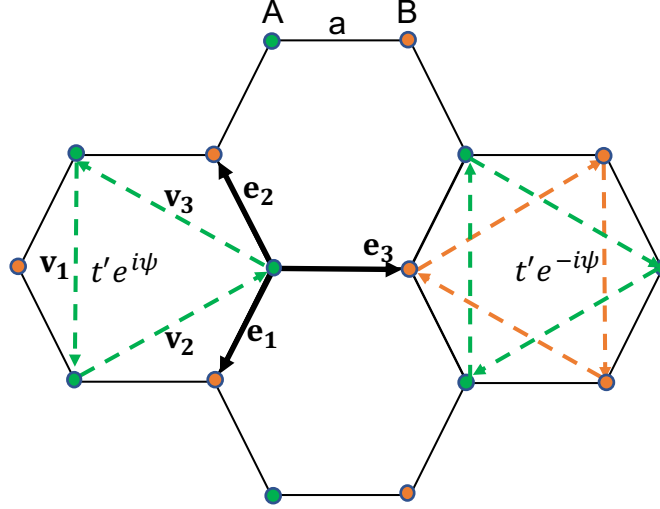


Figure 1. Hopping vectors and parameters for the Haldane Hamiltonian. Because of the complexified hopping, t' in Eq. (3), there is a net magnetic flux in each triangle which cancels out when averaged over the hexagon.

Of course there are instances in which topology and interactions merge as in the fractional^{14,15} quantum Hall effect (FQHE). Here, no single-particle description can encode the fractional charge or statistics of the quasiparticles in the fractional regime of the QHE. However, while it is the interactions that mediate the FQHE, the gap is set by the magnetic field rather than the interactions as in traditional Mott insulators. Recently, numerous examples have arisen of fractional Chern insulators in which features of the FQHE arise in the absence of Landau levels^{16–18}. In such systems, gaps^{16–18} open at fractional fillings and are set by the interaction strength. Such gaps seem to only arise in the flat-band limit in which the $\Delta \gg U$ (or V) $\gg W$, where Δ is the non-interacting topological gap, U the interaction strength and W the bandwidth. Hence, a key question arises: outside the flat-band limit, are there general cases of interaction-driven topological phases? Such cases would provide an analogue of a Mott insulator driven by the strong correlations but with topological signatures, for example a non-zero Chern number.

To achieve our goal of finding a topological Mott insulator, we put interactions into the spinful Haldane model¹ of topological insulators. In so doing, we uncover an overlooked phase at 1/4-filling which is a Mott insulator with a gap set by the non-trivial topology of the Haldane model. Prior work revealing inter-relations between Mott physics and topology has employed perturbative methods on models with spin-orbit and Hubbard-type interactions¹⁹, mean-field theory on near-neighbor and Hubbard interactions on a honeycomb lattice (with real hopping matrix elements)²⁰, models with band-touching in 3-dimensions²¹

and even bosonic systems²². Our work here is focused on making exact statements regardless of filling. Just as topological insulation can be thought of as a completion of band structure by the inclusion of spin-orbit, our work here on topological Mott insulation away from half-filling is a natural outgrowth of putting interactions into the spinful Haldane model. To this end, we consider two types of interactions, one local in momentum space as in the Hatsugai-Kohomoto (HK) model³ and the other local in position, the Hubbard interaction. While these interactions are extremes of one another, they both share a key ingredient. Namely, they both break the local-in-momentum space \mathbb{Z}_2 symmetry of a Fermi surface. That is, electrons on a Fermi surface are invariant^{5,23} to an interchange of particles and holes for a single spin species: $c_{p\uparrow} \rightarrow c_{p\uparrow}^\dagger$. Here, $c_{\mathbf{p}\sigma}^\dagger$ ($c_{\mathbf{p}\sigma}$) creates (annihilates) an electron with momentum \mathbf{p} and spin σ . Interactions, in general, do not preserve this symmetry and hence the breaking of the \mathbb{Z}_2 symmetry is a tell-tale sign that interactions are the root cause of the well known phenomenon of particle-hole asymmetry^{24–28} in the particle-addition and removal spectrum widely observed in correlated electron systems. To further buttress our previous arguments⁵ that breaking this symmetry establishes a fixed point and hence the nature of the interactions which accomplishes this is irrelevant, we show that essentially the same results obtain for the Hubbard as well as the HK models. We show explicitly that interactions induce a topologically non-trivial Mott insulating phase at quarter filling in the Haldane model for both the HK and Hubbard models. The advantage of the HK model is that all the calculations can be performed analytically. Our result then constitutes the first example of an exact demonstration of a topological phase driven by interactions. From the DQMC calculations with the Hubbard interaction, we are able to show that ferromagnetic order obtains in the quarter- and three-quarter-filled Haldane-Hubbard model.

2 Exactly solvable model for interacting Chern insulators

For spinful electrons, the Haldane model¹ with the hoppings designated in Fig. 1 takes a simple form

$$H = \sum_{\mathbf{k}, \sigma} [(\varepsilon_{+, \mathbf{k}} - \mu)n_{+, \mathbf{k}\sigma} + (\varepsilon_{-, \mathbf{k}} - \mu)n_{-, \mathbf{k}\sigma}], \quad (1)$$

in momentum space. Here μ is the chemical potential and

$$\varepsilon_{\pm, \mathbf{k}} = h_0(\mathbf{k}) \pm \sqrt{h_x^2(\mathbf{k}) + h_y^2(\mathbf{k}) + h_z^2(\mathbf{k})} \quad (2)$$

with

$$\begin{aligned} h_0(\mathbf{k}) &= -2t' \cos \psi \left[\sum_{i=1}^3 \cos(\mathbf{k} \cdot \mathbf{v}_i) \right], \\ h_x(\mathbf{k}) &= -t \left[\sum_{i=1}^3 \cos(\mathbf{k} \cdot \mathbf{e}_i) \right], \\ h_y(\mathbf{k}) &= -t \left[\sum_{i=1}^3 \sin(\mathbf{k} \cdot \mathbf{e}_i) \right], \\ h_z(\mathbf{k}) &= M - 2t' \sin \psi \left[\sum_{i=1}^3 \sin(\mathbf{k} \cdot \mathbf{v}_i) \right], \end{aligned} \quad (3)$$

representing the Haldane upper (+) and lower (−) bands. As depicted in Fig. 1, t and t' stand for the first and second neighbor hopping respectively, \mathbf{e}_i and \mathbf{v}_i are the bonding vectors for nearest neighbors and next nearest neighbors respectively, M is the Semenoff²⁹ mass. The hopping parameters are shown in Fig. 1. As is well known¹, the half-filled system is a topological insulator with Chern number $C = \pm 2$ (due to spin degeneracy) when $|M| < 3\sqrt{3}|t' \sin \psi|$ or a topologically trivial insulator with Chern number $C = 0$ when $|M| > 3\sqrt{3}|t' \sin \psi|$. Consequently, the gap between the degenerate spinful Haldane upper and lower bands is set by $\Delta = \min(6\sqrt{3}t' \sin \psi, 2)$ for small t' . The existence of non-trivial topology at half-filling is also shared with the model studied by Pesin and Balents¹⁹.

We now introduce interactions in the spirit of Hatsugai-Kohmoto (HK) interaction³⁻⁵ leading to the Hamiltonian,

$$\begin{aligned} H &= \sum_{\mathbf{k}, \sigma} [(\varepsilon_{+, \mathbf{k}} - \mu) n_{+, \mathbf{k}\sigma} + (\varepsilon_{-, \mathbf{k}} - \mu) n_{-, \mathbf{k}\sigma}] \\ &+ U \sum_{\mathbf{k}} (n_{+, \mathbf{k}\uparrow} n_{+, \mathbf{k}\downarrow} + n_{-, \mathbf{k}\uparrow} n_{-, \mathbf{k}\downarrow}), \end{aligned} \quad (4)$$

describing interacting electrons in the Haldane model. The primary role played by the interaction is to lift the \mathbb{Z}_2 symmetry of the non-interacting Fermi surfaces. What this effectively does is introduce Mottness

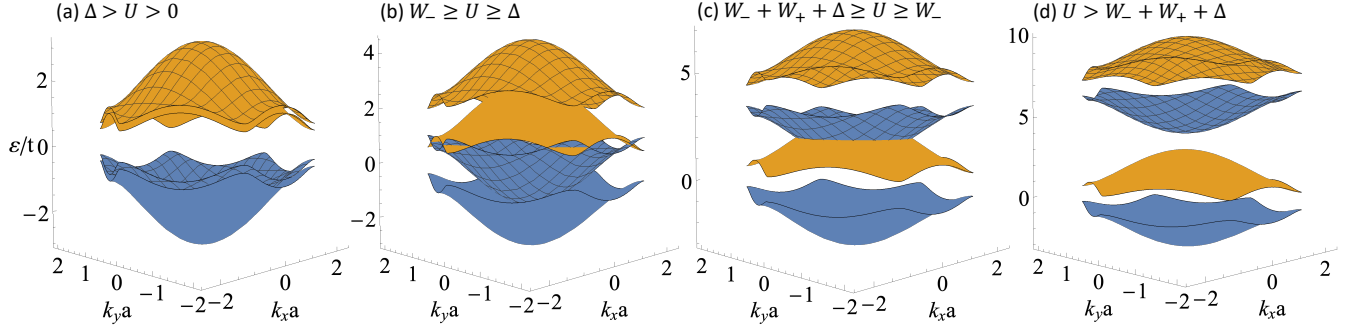


Figure 2. Band structure for the Haldane-HK model in Eq. (4) with $t'/t = 0.1$, $\psi = -\pi/2$, $M = 0$ at zero temperature. $\Delta \approx 1.04t$ is the non-interacting topological gap. $W_{+(-)} \approx 2.48t$ correspond to the bandwidth of the Haldane upper (lower) band. Different phases evolve as the interaction strength increases: (a) 1/2-filled topological insulator for $\Delta > U > 0$ ($U/t = 0.2$), (b) a metal for $W_- \geq U \geq \Delta$ ($U/t = 1.5$), (c) 1/4-filled Mott insulator with non-zero Chern number for $W_- + W_+ + \Delta \geq U \geq W_-$ ($U/t = 4$), and (d) 1/4-filled insulator for $U > W_- + W_+ + \Delta$ ($U/t = 7$). The blue (or orange) color represents Chern number $C = -1$ (or 1). The meshed band consists of only doubly occupied states, while the unmeshed band is singly occupied.

in the form of singly occupied states below the chemical potential. It is a simplicity of the HK model that such strong correlation is introduced without mixing the original non-interacting eigenstates. As a result, momentum \mathbf{k} is still a good quantum number and the Green function can be written down immediately⁴ as

$$G_{\pm, \mathbf{k}\sigma}(i\omega_n) \equiv - \int_0^\beta d\tau \langle c_{\pm, \mathbf{k}\sigma}(\tau) c_{\pm, \mathbf{k}\sigma}^\dagger(0) \rangle e^{i\omega_n \tau} \quad (5)$$

$$G_{\pm, \mathbf{k}\sigma}(i\omega_n \rightarrow \omega) = \frac{1 - \langle n_{\pm, \mathbf{k}\bar{\sigma}} \rangle}{\omega - \varepsilon_{\pm, \mathbf{k}}} + \frac{\langle n_{\pm, \mathbf{k}\bar{\sigma}} \rangle}{\omega - (\varepsilon_{\pm, \mathbf{k}} + U)}.$$

From the Green function, we see immediately the effect of the correlations. Each of the lower, $\varepsilon_{-, \mathbf{k}}$ and upper bands, $\varepsilon_{+, \mathbf{k}}$ will now be split into a singly and doubly occupied subband. Since, there is already a topological gap at half-filling, in the presence of interactions as the doubly occupied bands move up in energy, the singly-occupied bands can never get closer than Δ . Hence, at quarter-filling, a gap obtains and the non-trivial topology of the Haldane bands persists. It is the emergence of 1/4-filled Mott insulating states in a system that has a topologically engineered gap at half-filling that is the principal conclusion of this paper. To see how this state of affairs plays out, we plot the band structure in Eq. (5). As an example, we set $t'/t = 0.1$, $\psi = -\pi/2$, $M = 0$ without loss of generality so that the Haldane lower (upper) band has a Chern number $C = -1$ ($+1$) for each spin and hence the non-interacting half-filled system is a topological insulator with Chern number $C = -2$. We use $W_{+(-)}$ for the bandwidth of the Haldane

upper (lower) band and Δ for the Haldane gap. For this parameter set, $W_+ = W_- > \Delta$. Turning on U now results in four different phases for different interaction strengths, all of which are shown in Fig. 2. The blue and orange bands carry Chern $C = -1$ and $C = 1$, respectively. The interaction U only affects bands with the same color, making the blue and orange bands split into a singly occupied lower subband (unmeshed) and doubly occupied upper subband (meshed). However, the energy separation between the two unmeshed orange and blue bands remains fixed. This leads to a non-trivial interplay between topology and interaction strength. In Fig. 2(a) when U is small, the non-interacting band structure is mostly intact, and the system is a topological insulator at half-filling with Chern number $C = -2$. Increasing U to $W_- \geq U \geq \Delta$ as shown in Fig. 2(b) leads to a conductor with no gap for any density other than in the empty or full band limits. Increasing U further to $W_- + W_+ + \Delta \geq U > W_-$ as shown in Fig. 2(c), so that the two unmeshed singly occupied bands have no overlap with their doubly occupied same-color meshed-partners, results in a gap opening at $1/4$ - and $3/4$ -filling. While it is interactions that lead to a splitting of the bands, it is topology that dictates the separation between the two unlike-colored bands (meshed or otherwise). Consequently, the gap at $1/4$ - and $3/4$ -filling is set by the Haldane gap, Δ . The Chern number in either case is $C = -1$ and hence, this strongly correlated non-metallic state is actually a topological Mott insulator. Note at quarter-filling, the system consists of only singly occupied states as a result of strong correlation. We will resort to a Hubbard interaction to settle the nature of the spin correlations. Now consider increasing U further so that $U > W_- + W_+ + \Delta$. While the situation for $1/4$ - and $3/4$ -filling remains qualitatively unchanged, a gap opens at half-filling and the system at this density becomes a topologically trivial Mott insulator with only singly occupied states and Chern number $C = 0$. Although the features might change quantitatively in Fig. 2(b) and (c) for intermediate values of U with a different parameter set (t', ψ, M) , Fig. 2(d) is generally true for all parameters. This means when the correlation is strong enough, the system becomes an insulator at $1/4$ - and $3/4$ -filling with Chern number $C = C_0/2$ where C_0 is the Chern number at half-filling without interaction, and a topologically trivial insulator at half-filling with $C = 0$. Consequently, from the Hamiltonian Eq. (4), we are able to analytically describe the transition from a metal to a quarter-filled topological Mott insulator should U be the dominant energy scale. This constitutes the first analytically solvable model for the onset of topological phases in the presence of interactions. While Eq. (4) is in the parameters (t', ϕ, M) -dependent Haldane orbital basis,

it is also possible to write down an analytically solvable Hamiltonian in sub-lattice basis that contains essentially the same physics for strong interaction (see supplement). Due to its simplicity, we refer Eq. (4) as the analytically solvable Hamiltonian for interacting Haldane electrons. Note in the previous work, topologically induced interacting phases emerged only in the flat-band limit^{17,18}. Fig. 2 illustrates that no such constraint is necessary for the 1/4 or 3/4-filled topological insulating phases. As a final note, it is worth pointing out that topological states in the 1/4- and 3/4-filling in the Kitaev-Hubbard models³⁰ exist already in the non-interacting system and are impervious to interactions. What is new here is that the interactions induce a topological Mott insulator at 1/4- and 3/4-filling without affecting any details of the topology.

3 Numerical study on Haldane-Hofstadter-Hubbard model

It is natural to ask whether these conclusions persist in the more traditional Haldane-Hubbard model. Previous numerical studies³¹⁻³⁴ on the Haldane-Hubbard model focused mostly on the half-filling cases and showed a transition from a topological insulator to a topologically trivial Mott insulator. However, the region away from half-filling has rarely been explored. The deep question arises: do the 1/4- and 3/4-filled insulating states still appear when the interaction term mixes the orbitals that comprise the Haldane topological bands? The interaction used previously preserves the Haldane basis and hence, all it can do is to move the doubly occupied states up, keeping the distance between the singly occupied (unmeshed) sectors the same. What we want to show here is that the same conclusion is true for the Hubbard model.

The Hamiltonian for the Haldane-Hofstadter-Hubbard model is

$$H = - \sum_{ij\sigma} t_{i,j} \exp(i\phi_{i,j}) c_{i\sigma}^\dagger c_{j\sigma} - \mu \sum_{i,\sigma} n_{i\sigma} + M \sum_{i_A, i_B, \sigma} (n_{i_A\sigma} - n_{i_B\sigma}) + U \sum_i (n_{i\uparrow} - \frac{1}{2})(n_{i\downarrow} - \frac{1}{2}), \quad (6)$$

where $t_{i,j}$ represents the nearest neighbor hopping t (set to 1 as the energy scale) and next nearest neighbor hopping $t'e^{\pm i\psi}$, $i_{A(B)}$ means the lattice sites in the A (or B) sublattice, as shown in Fig. 1. Throughout this study, we set the Haldane phase $\psi = -\pi/2$ without loss of generality. Due to the presence of an external

uniform magnetic field, we use the Peierls substitution³⁵ to introduce the phase through the flux threading,

$$\phi_{\mathbf{i},\mathbf{j}} = \frac{2\pi}{\Phi_0} \int_{r_{\mathbf{i}}}^{r_{\mathbf{j}}} \mathbf{A} \cdot d\mathbf{l}, \quad (7)$$

where $\phi_0 = h/e$ represents the magnetic flux quantum and the integration is over the straight line path from site \mathbf{i} to \mathbf{j} . Here we apply an external magnetic field to measure the Chern number of the incompressible states at high temperature. As we will see, all the notable features are present (and stronger) for the smallest fluxes, thereby minimizing the effect of the external field which computationally reduces the finite size effects³⁶ at low temperature.

We use the DQMC method^{37–39} to simulate this model on an $N_{\text{site}} = 6 \times 6 \times 2$ cluster. The factor of 2 accounts for the two sublattices in the honeycomb lattice. The modified periodic boundary conditions in Ref. [40] are adjusted for the honeycomb lattice³⁶. The flux quantization condition $\Phi/\Phi_0 = n_f/N_c$ (with n_f an integer and N_c the number of unit cells) needs to be fulfilled for a single-value wave function. We choose the symmetric gauge $\mathbf{A} = (x\hat{y} - y\hat{x})B/2$ for this calculation. Due to the Fermionic sign problem, we focus on the inverse temperature $\beta = 3/t$ and vary other parameters t', M, U .

To analyze the phases that emerge, we study the charge compressibility

$$\chi = \beta \chi_c = \frac{\beta}{N} \sum_{\mathbf{i},\mathbf{j}} [\langle n_{\mathbf{i}} n_{\mathbf{j}} \rangle - \langle n_{\mathbf{i}} \rangle \langle n_{\mathbf{j}} \rangle], \quad (8)$$

in the presence of Hubbard interactions, where χ_c is the charge correlation function as a function of external flux ϕ/ϕ_0 . The green features in Fig. 3 occur at integers satisfying the Diophantine equation

$$\langle n \rangle = r \frac{\phi}{\phi_0} + s, \quad (9)$$

in which $\langle n \rangle = \langle N_e \rangle / N_c$, r is an integer given by the inverse slope of the straight lines and s is the offset given by the intercept. r defines the Chern number. Limited by the sign problem (see supplement), we work at relatively high temperature of $\beta = 3/t$. Panels Fig. 3(a) and (b) show the results for the compressibility of the non-interacting system. The green lines represent the leading minima in the charge compressibility and hence the intercept at vanishing flux represents the incompressible states at zero field. Note if we were

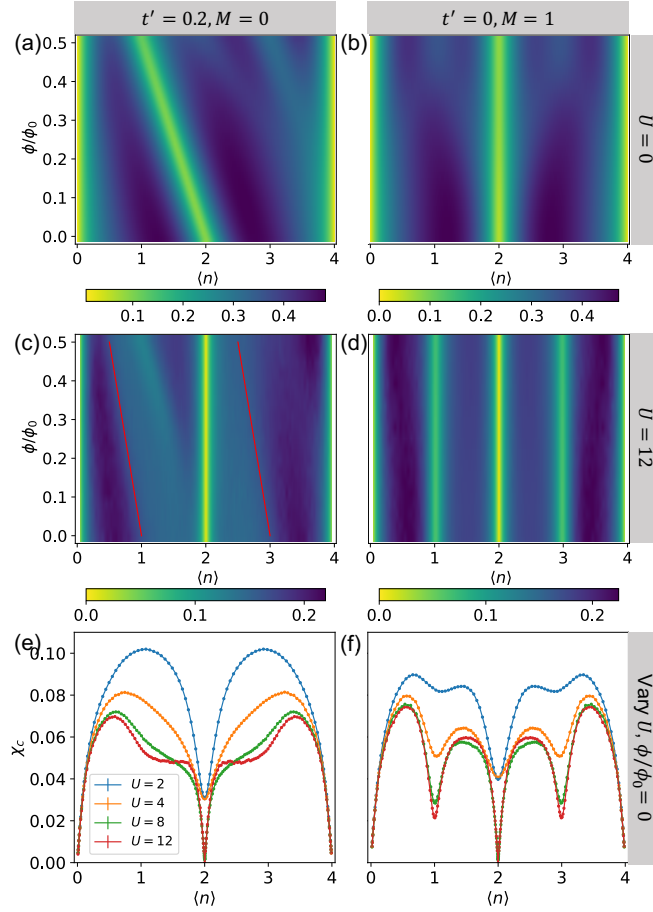


Figure 3. Compressibility χ as a function of magnetic flux and electron density in a $N_{\text{site}} = 6 \times 6 \times 2$ cluster for panel (a-d). The parameters are (a,c,e) $t'/t = 0.2, M = 0$ and (b,d,f) $t'/t = 0, M = 1$. The first and second rows are for the non-interacting and interacting ($U/t = 12$) systems, respectively. The third row shows the charge correlation $\chi_c = \chi/\beta$ at zero external magnetic flux for different interaction strength U . The temperature for all cases is $\beta = 3/t$.

to lower the temperature, a panoply of quantum Hall states would emerge which are not relevant to the study here as we are focused on the true zero-field features. As expected in the non-interacting case, the slope vanishes unless the complexified hopping $t' \neq 0$. In both cases, the green line interpolates to an incompressible state at half-filling, $\langle n \rangle = 2$. For $t' = 0.2, M = 0$, once strong interactions are turned on, new insulating states indicated by the valleys labeled by red lines in Fig. 3 (c) appear. They connect to $\langle n \rangle = 1$ and $\langle n \rangle = 3$, that is, $1/4$ - and $3/4$ -filling at zero field. The slope of the red lines gives a Chern number $C = -1$, while at $1/2$ -filling, the vertical green line gives $C = 0$ for a topologically trivial Mott insulator. For $t' = 0, M = 1$, strong correlation also introduce new insulating states at $1/4$ - and $3/4$ -filling, but all the insulating states have vanishing Chern numbers as evidenced by the three vertical lines in Fig. 3

(d). Panels Fig. 3 (e) and (f) represent a slice through (c) and (d) at zero flux, $\phi/\phi_0 = 0$. We see clearly that as the Hubbard interaction increases, the features outlined by the red line in (c) turn into distinct dips for both $t' \neq 0$ and for the topologically trivial case, $t' = 0$. This trend is more sharply apparent in Fig. 3 (f), however. This state of affairs obtains because the Hubbard interaction mixes the Haldane basis for $t' \neq 0, M = 0$ but not the sublattice states generated from $t' = 0, M \neq 0$. Nonetheless, in both cases the dips in the charge compressibility, which decrease as the temperature is lowered, are consistent with incompressible states at 1/4- and 3/4-filling.

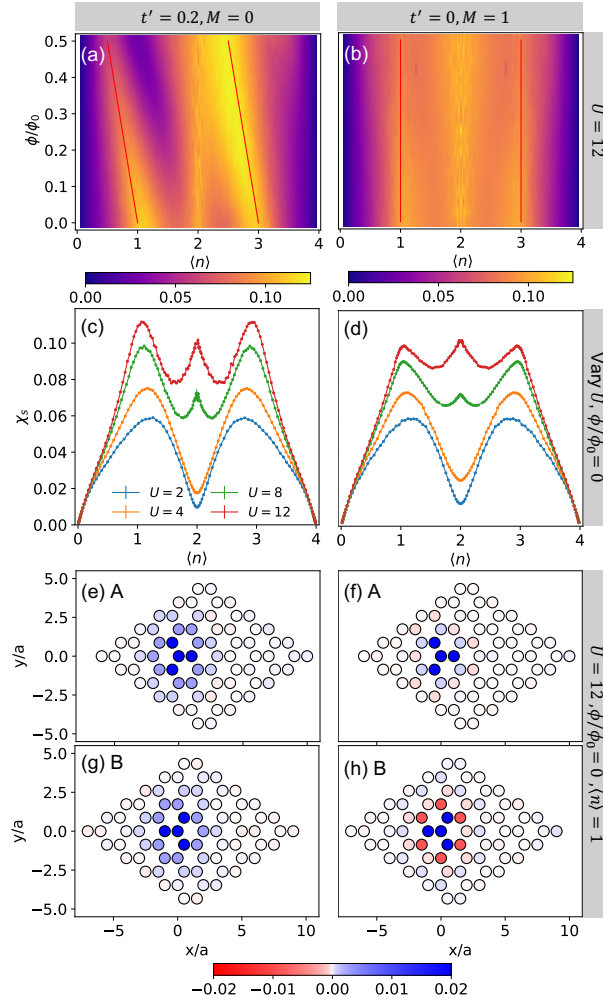


Figure 4. Spin correlation as a function of magnetic flux and electron density in a $N_{\text{site}} = 6 \times 6 \times 2$ cluster for panel (a,b). The parameters are (a,c,e,g) $t'/t = 0.2, M = 0$ and (b,d,f,h) $t'/t = 0, M/t = 1$. The second row shows the spin correlation at zero external magnetic flux for varying interaction strength, U . The third and fourth rows show the real-space zero-frequency spin susceptibility pattern at 1/4-filling $\langle n \rangle = 1$ from the perspective of the A and B sublattices, respectively. The temperature is $\beta = 3/t$ for all panels.

The only unresolved problem now is the nature of the spin correlations in the ground state. To this end,

we compute the spin correlation,

$$\chi_s = \sum_{m,n,\mathbf{r}} S_{m,n}(\mathbf{r}) = \frac{1}{N} \sum_{m,n,\mathbf{r}} \sum_{\mathbf{i}_m, \mathbf{i}_n} \langle S_{\mathbf{i}_m+\mathbf{r}}^z S_{\mathbf{i}_n}^z \rangle, \quad (10)$$

where $m, n = A, B$ and \mathbf{r} represents the vector delineating the unit cell. Panels Fig. 4(a) and (b) show the spin correlation results for the same systems as in Fig. 3(c) and (d), respectively. At 1/4- and 3/4-filling, we see distinct peaks in the spin correlation indicating a possible tendency for ferromagnetic alignment. From panel Fig. 4(a), we see that the slope is consistent with a non-zero Chern number of $C = -1$ at 1/4- and 3/4-filling. When $t' = 0$, vertical lines obtain signalling a vanishing of the Chern number. Fig. 4(c) and (d) show the spin correlation results for the same systems as in Fig. 4(e) and (f), respectively. In both panels (c) and (d), as U increases, a peak in spin correlation develops at 1/4-(or 3/4-)filling where a dip appears in the compressibility (charge correlation). Note although a peak also appears at half filling for large $U = 8, 12$ in both panels, it turns into a dip at lower temperature since the half-filled system becomes antiferromagnetic (see supplement). Finally, to detail the spatial dependence of the spin correlation at 1/4-filling, we calculate the real-space zero-frequency spin susceptibility

$$S_{m,n}(\mathbf{r}, \omega = 0) = \frac{1}{N} \sum_{\mathbf{i}_m, \mathbf{i}_n} \int_0^\beta \langle S_{\mathbf{i}_m+\mathbf{r}}^z(\tau) S_{\mathbf{i}_n}^z(0) \rangle d\tau, \quad (11)$$

which is more sensitive to short-range fluctuating order at high temperature than the equal-time spin correlation in Eq. (10). We plot $S_{m,A}(\mathbf{r}, \omega = 0)$ and $S_{m,B}(\mathbf{r}, \omega = 0)$ in panel (e,g) respectively for $t' \neq 0, M = 0$ and panel (f,h) respectively for $t' = 0, M \neq 0$. The topologically non-trivial case, Fig. 4(e,g), reveals ferromagnetic correlations on both sublattices. Note that the ferromagnetic insulating state at 1/4-filling is different from the quantum Hall ferromagnetic states in Ref. [36] although they both come with an odd-integer Chern number and lifting of the spin degeneracy. Here the ferromagnetic insulator appears at zero field and the correlation decays with increasing flux, shown in Fig. 4(a), while the quantum Hall ferromagnetic states in Ref. [36] requires finite magnetic flux and vanishes as the flux decreases. In the topologically trivial case, we first note a distinct difference between panels Fig. 4(f) and (h), implying a lifting of the sublattice degeneracy. While panel (f) shows ferromagnetism, panel (h) exhibits something

more akin to a spin-density wave.

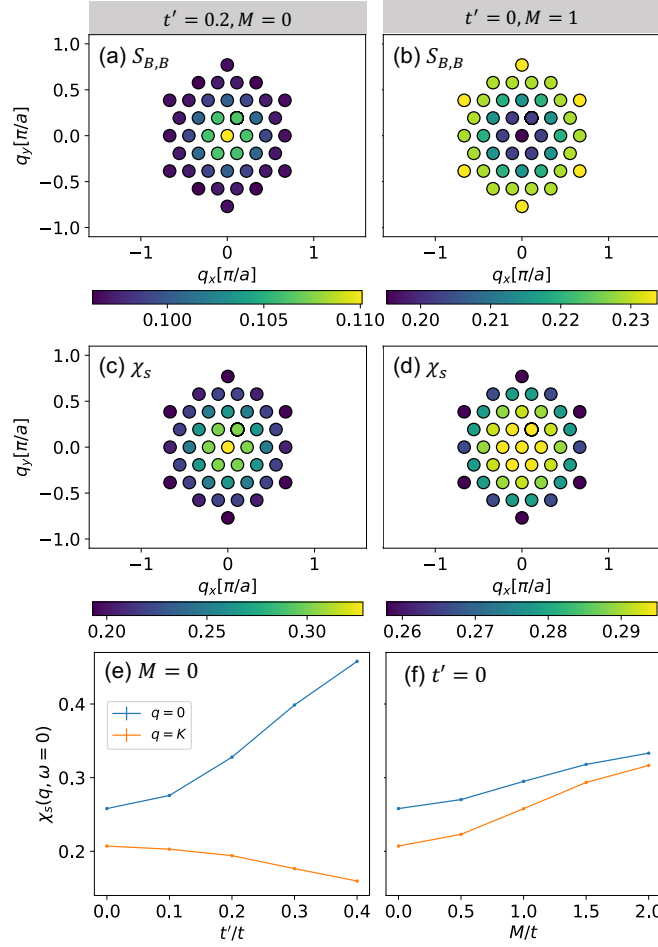


Figure 5. Zero-frequency spin susceptibility at quarter-filling. The first and second rows show the spin susceptibility pattern in momentum space $S_{B,B}(\mathbf{q}, \omega = 0)$ within the B sublattice and $\chi_s(\mathbf{q}, \omega = 0)$ summing over all sublattices for different parameter sets: (a) $t'/t = 0.2, M = 0$ and (b) $t'/t = 0, M = 1$. In the third row, panels (g) and (h) contain the zero-frequency spin susceptibility at $\mathbf{q} = 0$ and $\mathbf{q} = K$ as a function of t' (fixed $M = 0$) and M (fixed $t' = 0$), respectively. The other parameters are $U/t = 12$ and $\beta = 3/t$ for all panels.

To investigate this possibility further, we focus on the correlations in momentum space defined as

$$\begin{aligned}
 \chi_s(\mathbf{q}, \omega = 0) &= \sum_{m,n} S_{m,n}(\mathbf{q}, \omega = 0) \\
 &= \sum_{m,n} \sum_{\mathbf{r}} S_{m,n}(\mathbf{r}, \omega = 0) \exp[-i\mathbf{q} \cdot (\mathbf{r} + \Delta\mathbf{r}_{m,n})].
 \end{aligned} \tag{12}$$

This is displayed in Fig. 5. Specifically, we present $S_{B,B}(\mathbf{q}, \omega = 0)$ and $\chi_s(\mathbf{q}, \omega = 0)$ in the first and second rows, respectively. Panels Fig. 5 (a) and (c) show that regardless of the sublattice, the spin correlations are peaked at $\mathbf{q} = 0$ when $t' \neq 0, M = 0$. In Fig. 5 (e) as t' increases, the ferromagnetic ($\mathbf{q} = 0$) spin correlation is enhanced, while the correlation at the K point $K = (0, 4\pi/3\sqrt{3}a)$ dies out. Consequently, only $q = 0$ ferromagnetism survives in the ground state of the 1/4-filled state. This phenomenon is essentially the same for 3/4-filled state and as a consequence not shown. Alternatively, in the topologically trivial case, we find that within sublattice B, Fig. 5 (b) indicates that the spin susceptibility is peaked at the \mathbf{K} point and the symmetry related points in the Brillouin zone, while the other components $S_{A,A}$, $S_{A,B}$ and $S_{B,B}$ have a peak at $\mathbf{q} = 0$ (not presented). After summing over all the components, we see that $\chi_s(\mathbf{q}, \omega = 0)$ in Fig. 5 (d) reveals that the contributions at the K point and the center of the Brillouin zone are essentially equal at this temperature, given the short range in the color bar. Fig. 5 (h) shows that as M increases, the difference of spin correlation between the origin and K point becomes smaller, thereby showing no tendency for any particular order.

4 Experimental Realizations

Ultra-cold atom systems provide a natural venue to search for topological Mott physics due to the high degree of control over microscopic parameters they afford. In particular, such systems have been used to realize the non-interacting Haldane Hamiltonian including with spin mixtures⁴¹. Given the flexibility of this platform to effect fermionic interactions with tunable strength^{42,43}, a realization of the interacting Haldane model is in principle feasible. In addition, single layers of $\text{AFe}_2(\text{PO}_4)_2$ ($\text{A}=\text{Ba}, \text{Cs}, \text{K}, \text{La}$) have been shown⁴⁴ to be described by the Haldane model. However, because the spin bands are non-degenerate at the single-particle level, a pseudospin degree of freedom would be required to realize topological Mott physics, such as that offered by the three single-layer planes in the bulk unit cell. Finally we note that several moiré systems have been predicted^{45,46} and observed⁴⁷ to exhibit quantum anomalous Hall phases that map onto the spinless Haldane model. Stacking of two strongly interacting but electrically isolated copies of these superlattices, e.g. by twist decoupling or using a hexagonal boron nitride spacer whose thickness is small compared to the screening length, could also generate an effective layer pseudospin capable of supporting Mott physics in the topological bands.

5 Physical Interpretation: $4 = 1 + 1 + 1 + 1 \neq 2 + 2$

While there have been studies of the 1/4-filled Haldane-Hubbard model previously^{48,49}, none have disclosed both the topology and Mottness of that insulator. That quarter filling is ideally suited for Mottness follows from the 2-band nature of the Haldane model. Consider a non-topological system containing 2 atoms per unit cell. The ground state is now a band insulator in which the lower band is filled. If interactions are now added to this system, a Mott insulator ensues in the lower band at 1/4-filling of the lower band. It is for this reason that it matters not the form of the interactions, local-in momentum space or local-in real space, neither of which destroys the underlying topology of the Haldane bands. All that matters is that $4 = 1 + 1 + 1 + 1$. In a standard Mott insulator, the spectral weight at each k -point is split over two bands, the upper and lower Hubbard bands. In the topological Haldane model, each k -state is split over two bands. In the absence of interactions, each k -state can be doubly occupied with no energy cost, giving rise to $4 = 2 + 2$. When interactions are included, the singly and doubly occupied bands now have distinct energies as indicated by the 4 poles in the Green function, hence the equation $4 = 1 + 1 + 1 + 1 \neq 2 + 2$. The standard Mott picture consists just of two bands. Now, however, 4 bands exist each with equal spectral weight. The two lowest singly-occupied bands (unmeshed blue and orange in Fig. 2) remain singly occupied with a fixed energy separation of the topological gap Δ . As a result, the 1/4-filled state is gapped with non-trivial topological signature, $C = -1$. It is for this reason that the Hubbard-Haldane model yields the same results because Mott insulation in the presence of topology (at least that in the Haldane model) necessarily gives rise to 4 non-degenerate energy bands. Since these bands are inherently in momentum space, this suggests that Mott insulation is more easily understood in momentum space rather than in real space. At work here, as we have demonstrated⁵ all interactions break the local-in momentum space Z_2 symmetry of a Fermi liquid. The HK interaction is the simplest one that does this and hence suffices to explain the origin of topological Mott insulation. Undoubtedly, extensions of this work beyond the Haldane model exist. Nonetheless, this work provides a general framework for thinking about this new state of matter.

Acknowledgements

Supported by the Center for Quantum Sensing and Quantum Materials, a DOE Energy Frontier

Research Center, grant DE-SC0021238 (P.M. B. E. F., and P.W.P.) PWP also acknowledges NSF DMR-2111379 for partial funding of the HK work which led to these results and Srinivas Raghu for comments on an earlier draft. The DQMC calculation of this work used the Extreme Science and Engineering Discovery Environment (XSEDE) expense supercomputer through the research allocation TG-PHY220042, which is supported by National Science Foundation grant number ACI-1548562⁵⁰.

References

1. Haldane, F. D. M. Model for a quantum hall effect without landau levels: Condensed-matter realization of the "parity anomaly". *Phys. Rev. Lett.* **61**, 2015–2018, DOI: [10.1103/PhysRevLett.61.2015](https://doi.org/10.1103/PhysRevLett.61.2015) (1988).
2. Kane, C. L. & Mele, E. J. Z_2 topological order and the quantum spin hall effect. *Phys. Rev. Lett.* **95**, 146802, DOI: [10.1103/PhysRevLett.95.146802](https://doi.org/10.1103/PhysRevLett.95.146802) (2005).
3. Hatsugai, Y. & Kohmoto, M. Exactly solvable model of correlated lattice electrons in any dimensions. *J. Phys. Soc. Jpn.* **61**, 2056–2069, DOI: [10.1143/JPSJ.61.2056](https://doi.org/10.1143/JPSJ.61.2056) (1992). <https://doi.org/10.1143/JPSJ.61.2056>.
4. Phillips, P. W., Yeo, L. & Huang, E. W. Exact theory for superconductivity in a doped mott insulator. *Nat. Phys.* **16**, 1175–1180, DOI: [10.1038/s41567-020-0988-4](https://doi.org/10.1038/s41567-020-0988-4) (2020).
5. Huang, E. W., Nave, G. L. & Phillips, P. W. Discrete symmetry breaking defines the mott quartic fixed point. *Nat. Phys.* **18**, 511–516, DOI: [10.1038/s41567-022-01529-8](https://doi.org/10.1038/s41567-022-01529-8) (2022).
6. Laughlin, R. B. Quantized hall conductivity in two dimensions. *Phys. Rev. B* **23**, 5632–5633, DOI: [10.1103/PhysRevB.23.5632](https://doi.org/10.1103/PhysRevB.23.5632) (1981).
7. Fu, L., Kane, C. L. & Mele, E. J. Topological insulators in three dimensions. *Phys. Rev. Lett.* **98**, 106803, DOI: [10.1103/PhysRevLett.98.106803](https://doi.org/10.1103/PhysRevLett.98.106803) (2007).
8. Moore, J. E. & Balents, L. Topological invariants of time-reversal-invariant band structures. *Phys. Rev. B* **75**, 121306, DOI: [10.1103/PhysRevB.75.121306](https://doi.org/10.1103/PhysRevB.75.121306) (2007).
9. Murakami, S., Nagaosa, N. & Zhang, S.-C. Spin-hall insulator. *Phys. Rev. Lett.* **93**, 156804, DOI: [10.1103/PhysRevLett.93.156804](https://doi.org/10.1103/PhysRevLett.93.156804) (2004).

10. Roy, R. Integer quantum hall effect on a square lattice with zero net magnetic field, DOI: [10.48550/ARXIV.COND-MAT/0603271](https://doi.org/10.48550/ARXIV.COND-MAT/0603271).
11. Roy, R. Z_2 classification of quantum spin hall systems: An approach using time-reversal invariance. *Phys. Rev. B* **79**, 195321, DOI: [10.1103/PhysRevB.79.195321](https://doi.org/10.1103/PhysRevB.79.195321) (2009).
12. Bernevig, B. A., Hughes, T. L. & Zhang, S.-C. Quantum spin hall effect and topological phase transition in HgTe quantum wells. *Science* **314**, 1757–1761, DOI: [10.1126/science.1133734](https://doi.org/10.1126/science.1133734) (2006).
13. Thouless, D. J., Kohmoto, M., Nightingale, M. P. & den Nijs, M. Quantized hall conductance in a two-dimensional periodic potential. *Phys. Rev. Lett.* **49**, 405–408, DOI: [10.1103/PhysRevLett.49.405](https://doi.org/10.1103/PhysRevLett.49.405) (1982).
14. Laughlin, R. B. Anomalous quantum hall effect: An incompressible quantum fluid with fractionally charged excitations. *Phys. Rev. Lett.* **50**, 1395–1398, DOI: [10.1103/PhysRevLett.50.1395](https://doi.org/10.1103/PhysRevLett.50.1395) (1983).
15. Haldane, F. D. M. Fractional quantization of the hall effect: A hierarchy of incompressible quantum fluid states. *Phys. Rev. Lett.* **51**, 605–608, DOI: [10.1103/PhysRevLett.51.605](https://doi.org/10.1103/PhysRevLett.51.605) (1983).
16. Neupert, T., Santos, L., Chamon, C. & Mudry, C. Fractional quantum hall states at zero magnetic field. *Phys. Rev. Lett.* **106**, 236804, DOI: [10.1103/PhysRevLett.106.236804](https://doi.org/10.1103/PhysRevLett.106.236804) (2011).
17. Neupert, T., Santos, L., Ryu, S., Chamon, C. & Mudry, C. Fractional topological liquids with time-reversal symmetry and their lattice realization. *Phys. Rev. B* **84**, 165107, DOI: [10.1103/PhysRevB.84.165107](https://doi.org/10.1103/PhysRevB.84.165107) (2011).
18. Parameswaran, S. A., Roy, R. & Sondhi, S. L. Fractional quantum hall physics in topological flat bands. *Comptes Rendus Physique* **14**, 816–839, DOI: <https://doi.org/10.1016/j.crhy.2013.04.003> (2013). Topological insulators / Isolants topologiques.
19. Pesin, D. & Balents, L. Mott physics and band topology in materials with strong spin–orbit interaction. *Nat. Phys.* **6**, 376–381, DOI: [10.1038/nphys1606](https://doi.org/10.1038/nphys1606) (2010).
20. Raghu, S., Qi, X.-L., Honerkamp, C. & Zhang, S.-C. Topological mott insulators. *Phys. Rev. Lett.* **100**, 156401, DOI: [10.1103/PhysRevLett.100.156401](https://doi.org/10.1103/PhysRevLett.100.156401) (2008).

21. Herbut, I. F. & Janssen, L. Topological mott insulator in three-dimensional systems with quadratic band touching. *Phys. Rev. Lett.* **113**, 106401, DOI: [10.1103/PhysRevLett.113.106401](https://doi.org/10.1103/PhysRevLett.113.106401) (2014).
22. Kuno, Y., Shimizu, K. & Ichinose, I. Various topological mott insulators and topological bulk charge pumping in strongly-interacting boson system in one-dimensional superlattice. *New J. Phys.* **19**, 123025, DOI: [10.1088/1367-2630/aa99d0](https://doi.org/10.1088/1367-2630/aa99d0) (2017).
23. Anderson, P. W. & Haldane, F. D. M. The symmetries of fermion fluids at low dimensions. *J. Stat. Phys.* **103**, 425–428, DOI: [10.1023/A:1010324912515](https://doi.org/10.1023/A:1010324912515) (2001).
24. Hanaguri, T. *et al.* A ‘checkerboard’ electronic crystal state in lightly hole-doped $\text{Ca}_{2-x}\text{Na}_x\text{CuO}_2\text{Cl}_2$. *Nature* **430**, 1001–1005, DOI: [10.1038/nature02861](https://doi.org/10.1038/nature02861) (2004).
25. Miller, T. L., Zhang, W., Eisaki, H. & Lanzara, A. Particle-hole asymmetry in the cuprate pseudogap measured with time-resolved spectroscopy. *Phys. Rev. Lett.* **118**, 097001, DOI: [10.1103/PhysRevLett.118.097001](https://doi.org/10.1103/PhysRevLett.118.097001) (2017).
26. Anderson, P. & Ong, N. Theory of asymmetric tunneling in the cuprate superconductors. *J. Phys. Chem. Solids* **67**, 1–5, DOI: <https://doi.org/10.1016/j.jpcs.2005.10.132> (2006). Spectroscopies in Novel Superconductors 2004.
27. Maiti, K., Singh, R. S. & Medicherla, V. R. R. Observation of particle hole asymmetry and phonon excitations in non-fermi-liquid systems: A high-resolution photoemission study of ruthenates. *Europhys. Lett. (EPL)* **78**, 17002, DOI: [10.1209/0295-5075/78/17002](https://doi.org/10.1209/0295-5075/78/17002) (2007).
28. Yu, Y. *et al.* High-temperature superconductivity in monolayer $\text{Bi}_2\text{Sr}_2\text{CaCu}_2\text{O}_{8+\delta}$. *Nature* **575**, 156–163, DOI: [10.1038/s41586-019-1718-x](https://doi.org/10.1038/s41586-019-1718-x) (2019).
29. Semenoff, G. W. Condensed-matter simulation of a three-dimensional anomaly. *Phys. Rev. Lett.* **53**, 2449–2452, DOI: [10.1103/PhysRevLett.53.2449](https://doi.org/10.1103/PhysRevLett.53.2449) (1984).
30. Hassan, S. R., Goyal, S., Shankar, R. & Sénéchal, D. Quarter-filled kitaev-hubbard model: A quantum hall state in an optical lattice. *Phys. Rev. B* **88**, 045301, DOI: [10.1103/PhysRevB.88.045301](https://doi.org/10.1103/PhysRevB.88.045301) (2013).
31. Vanhala, T. I. *et al.* Topological phase transitions in the repulsively interacting haldane-hubbard model. *Phys. Rev. Lett.* **116**, 225305, DOI: [10.1103/PhysRevLett.116.225305](https://doi.org/10.1103/PhysRevLett.116.225305) (2016).

32. Shao, C., Castro, E. V., Hu, S. & Mondaini, R. Interplay of local order and topology in the extended haldane-hubbard model. *Phys. Rev. B* **103**, 035125, DOI: [10.1103/PhysRevB.103.035125](https://doi.org/10.1103/PhysRevB.103.035125) (2021).
33. Imriška, J., Wang, L. & Troyer, M. First-order topological phase transition of the haldane-hubbard model. *Phys. Rev. B* **94**, 035109, DOI: [10.1103/PhysRevB.94.035109](https://doi.org/10.1103/PhysRevB.94.035109) (2016).
34. Mertz, T., Zantout, K. & Valentí, R. Statistical analysis of the chern number in the interacting haldane-hubbard model. *Phys. Rev. B* **100**, 125111, DOI: [10.1103/PhysRevB.100.125111](https://doi.org/10.1103/PhysRevB.100.125111) (2019).
35. Peierls, R. Zur theorie des diamagnetismus von leitungselektronen. *Zeitschrift für Physik* **80**, 763–791, DOI: [10.1007/BF01342591](https://doi.org/10.1007/BF01342591) (1933).
36. Mai, P., Huang, E. W., Yu, J., Feldman, B. E. & Phillips, P. W. Interaction-driven spontaneous ferromagnetic insulating states with odd chern numbers, DOI: [10.48550/ARXIV.2205.08545](https://doi.org/10.48550/ARXIV.2205.08545) (2022).
37. Blankenbecler, R., Scalapino, D. J. & Sugar, R. L. Monte carlo calculations of coupled boson-fermion systems. i. *Phys. Rev. D* **24**, 2278–2286, DOI: [10.1103/PhysRevD.24.2278](https://doi.org/10.1103/PhysRevD.24.2278) (1981).
38. Hirsch, J. E. Two-dimensional hubbard model: Numerical simulation study. *Phys. Rev. B* **31**, 4403–4419, DOI: [10.1103/PhysRevB.31.4403](https://doi.org/10.1103/PhysRevB.31.4403) (1985).
39. White, S. R. *et al.* Numerical study of the two-dimensional hubbard model. *Phys. Rev. B* **40**, 506–516, DOI: [10.1103/PhysRevB.40.506](https://doi.org/10.1103/PhysRevB.40.506) (1989).
40. Assaad, F. F. Depleted kondo lattices: Quantum monte carlo and mean-field calculations. *Phys. Rev. B* **65**, 115104, DOI: [10.1103/PhysRevB.65.115104](https://doi.org/10.1103/PhysRevB.65.115104) (2002).
41. Jotzu, G. *et al.* Experimental realization of the topological haldane model with ultracold fermions. *Nature* **515**, 237–240, DOI: [10.1038/nature13915](https://doi.org/10.1038/nature13915) (2014).
42. Hart, R. A. *et al.* Observation of antiferromagnetic correlations in the hubbard model with ultracold atoms. *Nature* **519**, 211–214, DOI: [10.1038/nature14223](https://doi.org/10.1038/nature14223) (2015).
43. Esslinger, T. Fermi-hubbard physics with atoms in an optical lattice. *Annu. Rev. Condens. Matter Phys.* **1**, 129–152, DOI: [10.1146/annurev-conmatphys-070909-104059](https://doi.org/10.1146/annurev-conmatphys-070909-104059) (2010). <https://doi.org/10.1146/annurev-conmatphys-070909-104059>.

44. Kim, H.-S. & Kee, H.-Y. Realizing haldane model in fe-based honeycomb ferromagnetic insulators. *npj Quantum Mater.* **2**, 20, DOI: [10.1038/s41535-017-0021-z](https://doi.org/10.1038/s41535-017-0021-z) (2017).
45. Wu, F., Lovorn, T., Tutuc, E., Martin, I. & MacDonald, A. H. Topological insulators in twisted transition metal dichalcogenide homobilayers. *Phys. Rev. Lett.* **122**, 086402, DOI: [10.1103/PhysRevLett.122.086402](https://doi.org/10.1103/PhysRevLett.122.086402) (2019).
46. Zhang, Y.-H., Mao, D., Cao, Y., Jarillo-Herrero, P. & Senthil, T. Nearly flat chern bands in moiré superlattices. *Phys. Rev. B* **99**, 075127, DOI: [10.1103/PhysRevB.99.075127](https://doi.org/10.1103/PhysRevB.99.075127) (2019).
47. Li, T. *et al.* Quantum anomalous hall effect from intertwined moiré bands. *Nature* **600**, 641–646 (2021).
48. Leite, L. S. G. & Doretto, R. L. Flat-band ferromagnetism and spin waves in the haldane-hubbard model. *Phys. Rev. B* **104**, 155129, DOI: [10.1103/PhysRevB.104.155129](https://doi.org/10.1103/PhysRevB.104.155129) (2021).
49. Gu, Z.-L., Dong, Z.-Y., Yu, S.-L. & Li, J.-X. Itinerant topological magnons in haldane hubbard model with a nearly-flat electron band (2019). [1908.09255](https://arxiv.org/abs/1908.09255).
50. Towns, J. *et al.* Xsede: Accelerating scientific discovery. *Comput. Sci. Eng.* **16**, 62–74, DOI: [10.1109/MCSE.2014.80](https://doi.org/10.1109/MCSE.2014.80) (2014).

Topological Mott Insulator at Quarter Filling in the Interacting Haldane Model: supplementary information

Peizhi Mai¹, Ben Feldman^{2,3,4}, and Philip W. Phillips^{1,*}

¹Department of Physics and Institute of Condensed Matter Theory, University of Illinois at Urbana-Champaign, Urbana, IL 61801, USA

²Geballe Laboratory of Advanced Materials, Stanford, CA 94305, USA

³Department of Physics, Stanford University, Stanford, CA 94305, USA

⁴Stanford Institute for Materials and Energy Sciences, SLAC National Accelerator Laboratory, Menlo Park, CA 94025, USA

9 1 Hamiltonian with Interaction-Independent Basis

10 The analytically solvable Hamiltonian in Eq. (1) of the main text provides a simple model for the interacting
 11 Haldane electrons. However, the interaction term has a simple form (leading to the simple solution) only in
 12 the basis that diagonalizes the non-interacting Hamiltonian. This means that the interaction term depends
 13 on the choice of t' , ψ and M . The natural question is whether or not it is possible to write the interaction
 14 term in a similarly simple form independent of basis without surrendering the essential solution outlined
 15 in the text. The answer is yes. We can write the Hamiltonian as

$$H = \sum_{\mathbf{k}, \sigma} [(\varepsilon_{+, \mathbf{k}} - \mu)n_{+, \mathbf{k}\sigma} + (\varepsilon_{-, \mathbf{k}} - \mu)n_{-, \mathbf{k}\sigma}] + U' \sum_{\mathbf{k}} (n_{+, \mathbf{k}\uparrow} + n_{-, \mathbf{k}\uparrow})(n_{+, \mathbf{k}\downarrow} + n_{-, \mathbf{k}\downarrow}). \quad (1)$$

16 The quantity $n_{+, \mathbf{k}\sigma} + n_{-, \mathbf{k}\sigma}$ is a trace in the Haldane orbital space and is therefore independent of the
 17 orbital basis, that is, the interaction term is the same for all combinations of t' , ψ and M . This Hamiltonian
 18 is also analytically solvable, since the interaction does not mix the original non-interacting eigenstates.
 19 We can write the Green function as

$$\begin{aligned} G_{\pm, \mathbf{k}\sigma}(i\omega_n \rightarrow \omega) &= \frac{(1 - \langle n_{+, \mathbf{k}\bar{\sigma}} \rangle)(1 - \langle n_{-, \mathbf{k}\bar{\sigma}} \rangle)}{\omega - \varepsilon_{\pm, \mathbf{k}}} + \frac{(1 - \langle n_{+, \mathbf{k}\bar{\sigma}} \rangle)\langle n_{-, \mathbf{k}\bar{\sigma}} \rangle + (1 - \langle n_{-, \mathbf{k}\bar{\sigma}} \rangle)\langle n_{+, \mathbf{k}\bar{\sigma}} \rangle}{\omega - (\varepsilon_{\pm, \mathbf{k}} + U')} \\ &\quad + \frac{\langle n_{+, \mathbf{k}\bar{\sigma}} \rangle \langle n_{-, \mathbf{k}\bar{\sigma}} \rangle}{\omega - (\varepsilon_{\pm, \mathbf{k}} + 2U')} \\ &= \frac{(1 - \langle n_{+, \mathbf{k}\bar{\sigma}} \rangle)(1 - \langle n_{-, \mathbf{k}\bar{\sigma}} \rangle)}{\omega - \varepsilon_{\pm, \mathbf{k}}} + \frac{\langle n_{+, \mathbf{k}\bar{\sigma}} \rangle + \langle n_{-, \mathbf{k}\bar{\sigma}} \rangle - \langle n_{+, \mathbf{k}\bar{\sigma}} \rangle \langle n_{-, \mathbf{k}\bar{\sigma}} \rangle}{\omega - (\varepsilon_{\pm, \mathbf{k}} + U')} \\ &\quad + \frac{\langle n_{+, \mathbf{k}\bar{\sigma}} \rangle \langle n_{-, \mathbf{k}\bar{\sigma}} \rangle}{\omega - (\varepsilon_{\pm, \mathbf{k}} + 2U')}. \end{aligned} \quad (2)$$

20 At zero temperature with a large enough U' ($U' > W_+ + W_- + \Delta$), for each \mathbf{k} , the state with the same spin
 21 would be filled up first to avoid the cost of interaction energy. After that, the state with opposite spin
 22 would start to be filled with the interaction energy cost of $2U'$. In this sense, the band structure would be
 23 similar to that for the Hamiltonian in Eq. (1) of the main text if $U = 2U'$. Choosing the same example
 24 parameter set $t' = 0.1$, $\psi = -\pi/2$ and $M = 0$ ($W_+ + W_- + \Delta = 6$), we plot the band structure in Fig. 1
 25 (setting $U' = 8$). The system is a topological Mott insulator at 1/4- (or 3/4-) filling and a topologically

26 trivial Mott insulator at $1/2$ -filling. The band structure is almost the same as that in Fig. 2(d) of the main
 27 text if $U = 2U' = 16$. The only difference is that in Fig. 1 for Hamiltonian Eq. (1), once the lowest
 28 band is filled up, the states of the second lowest band are fixed with no degeneracy. For each \mathbf{k} , the state
 29 contains the same spin as that in the lowest band with the same momentum. In Fig. 2(d) of the main
 30 text, the degeneracy of the second lowest band remains with a full lowest band. In short, we construct a
 31 Hamiltonian Eq. (1) for interacting Haldane electrons independent of basis and containing essentially the
 32 same physics as Eq. (1) of the main text under strong correlation.

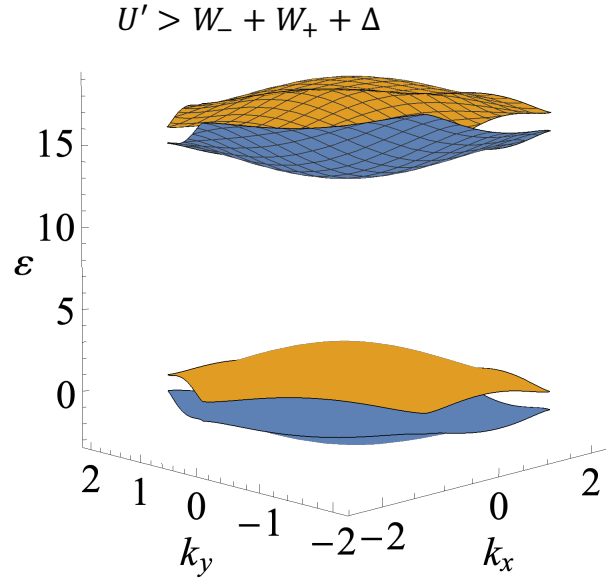


Figure 1. Band structure for the generalized Haldane-HK model in Eq. (1) with $t'/t = 0.1$, $\psi = -\pi/2$, $M = 0$ and $U' = 8 > W_+ + W_- + \Delta$. $\Delta = 6\sqrt{3}t' \sin \psi$ is the non-interacting topological gap. $W_{+(-)}$ correspond to the bandwidth of the Haldane upper (lower) band. The blue (or orange) color represents Chern number $C = -1$ (or 1). The meshed band consists of only doubly occupied states, while the unmeshed band is singly occupied.

2 Sign problem of determinantal quantum Monte-carlo simulation for the Haldane-Hubbard model

The determinantal quantum Monte-carlo (DQMC) simulation suffers from a fermionic sign problem when turning on the Hubbard interaction in the Haldane-Hubbard model. Generally, the average sign decays exponentially as the interaction strength increases or temperature decreases, leading to the exponential increase on the necessary number of measurements to bring down the error bar. For this reason, we are restricted at a relatively high temperature $\beta = 3$ while working with a large $U = 12$. The average sign varies largely along with the density, as shown in Fig. 2.

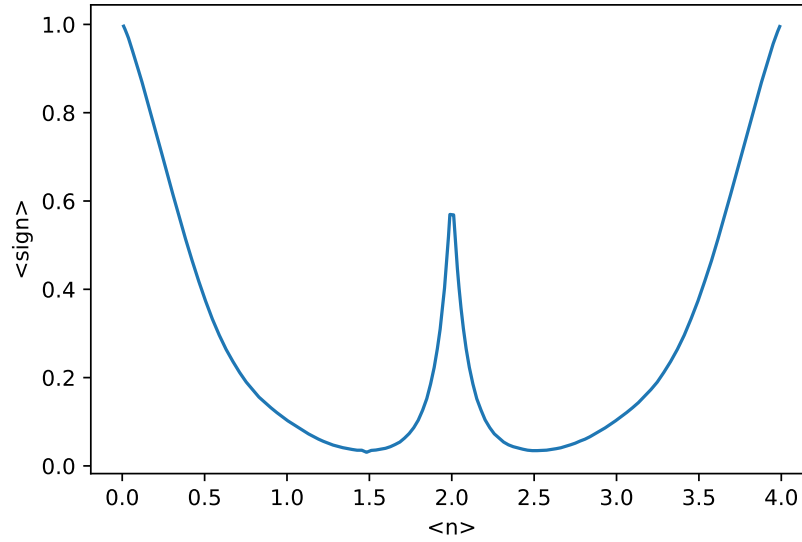


Figure 2. Average DQMC sign as a function of density for $t' = 0.2, M = 0, U = 12$ and $\beta = 3$ at zero magnetic flux.

3 Anti-ferromagnetism in the half-filled system

To explore the structure of spin correlation at half filling, the middle peak of Fig. 4 (c) and (d) in the main text, we calculate the zero-frequency spin susceptibility in real and momentum space:

$$S_{m,n}(\mathbf{r}, \omega = 0) = \frac{1}{N} \sum_{\mathbf{i}_m, \mathbf{i}_n} \int_0^\beta \langle S_{\mathbf{i}_m + \mathbf{r}}^z(\tau) S_{\mathbf{i}_n}^z(0) \rangle d\tau, \quad (3)$$

44

$$S_{m,n}(\mathbf{q}, \omega = 0) = \sum_{m,n} \sum_{\mathbf{r}} S_{m,n}(\mathbf{r}, \omega = 0) \exp[-i\mathbf{q} \cdot (\mathbf{r} + \Delta\mathbf{r}_{m,n})].. \quad (4)$$

The results are shown in Fig. 3 for the topologically nontrivial case ($t' = 0.2, M = 0$) and Fig. 4 for the topologically trivial case ($t' = 0, M = 1$) at $\beta = 3/t$ and $\beta = 5/t$. Note that the smallest magnetic flux $\phi/\phi_0 = 1/36$ is applied to reduce the finite size effects at lower temperature, and hence the conclusion can be extrapolated to zero field. In Fig. 3, the first row features $S_{m,B}(\mathbf{r}, \omega = 0)$ ($m = A, B$) indicating that anti-ferromagnetism develops as the temperature decreases. For strong anti-ferromagnetism, the spin correlation should be ferromagnetic in the intra-sublattice components and anti-ferromagnetic in the inter-sublattice components with the same amplitude. Therefore, we show $S_{B,B}(\mathbf{q}, \omega = 0)$ and $S_{A,B}(\mathbf{q}, \omega = 0)$ in the second and third rows, respectively. At $\beta = 3/t$, indeed $S_{B,B}(\mathbf{q}, \omega = 0)$ is ferromagnetic and $S_{A,B}(\mathbf{q}, \omega = 0)$ is anti-ferromagnetic. But the amplitude yields $|S_{A,B}(\mathbf{q} = 0, \omega = 0)| < |S_{B,B}(\mathbf{q} = 0, \omega = 0)|$ leading to a residual $\mathbf{q} = 0$ contribution in the total spin correlation corresponding to the middle peak in Fig. 3(c) in the main text. However, at a lower temperature $\beta = 5/t$, the amplitude becomes comparable $|S_{A,B}(\mathbf{q} = 0, \omega = 0)| \approx |S_{B,B}(\mathbf{q} = 0, \omega = 0)|$, resulting in a vanishing $\mathbf{q} = 0$ component for the total spin correction, as expected for anti-ferromagnetism. The situation is similar for the topologically trivial case in Fig. 4 except that now we are comparing the amplitude $|S_{A,B}(\mathbf{q} = 0, \omega = 0) + S_{B,A}(\mathbf{q} = 0, \omega = 0)|$ and $|S_{A,A}(\mathbf{q} = 0, \omega = 0) + S_{B,B}(\mathbf{q} = 0, \omega = 0)|$ due to the lifting of the sublattice degeneracy. Similarly, $S_{A,B}(\mathbf{q} = 0, \omega = 0) = S_{B,A}(\mathbf{q} = 0, \omega = 0)$ for symmetry reasons.

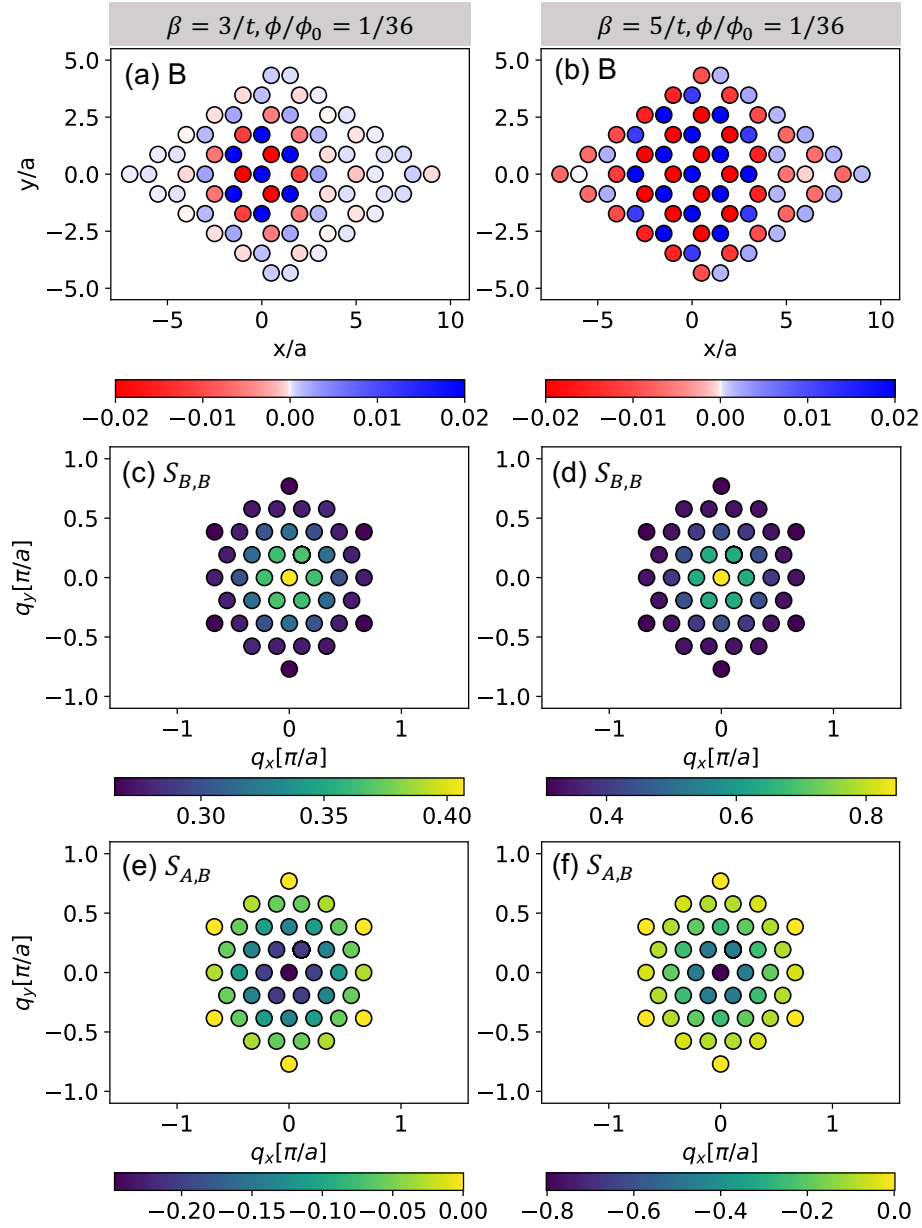


Figure 3. Zero-frequency spin susceptibility at half-filling for the topologically nontrivial case $t' = 0.2, M = 0$. The left and right columns show the susceptibility at the temperature $\beta = 3/t$ and $\beta = 5/t$, respectively. The first row features $S_{m,B}(\mathbf{r}, \omega = 0)$ ($m = A, B$) in real space. The second and third rows display $S_{B,B}(\mathbf{q}, \omega = 0)$ and $S_{A,B}(\mathbf{q}, \omega = 0)$ in momentum space, respectively. The interaction strength is $U/t = 12$ and the smallest magnetic flux $\phi/\phi_0 = 1/36$ is applied for all panels.

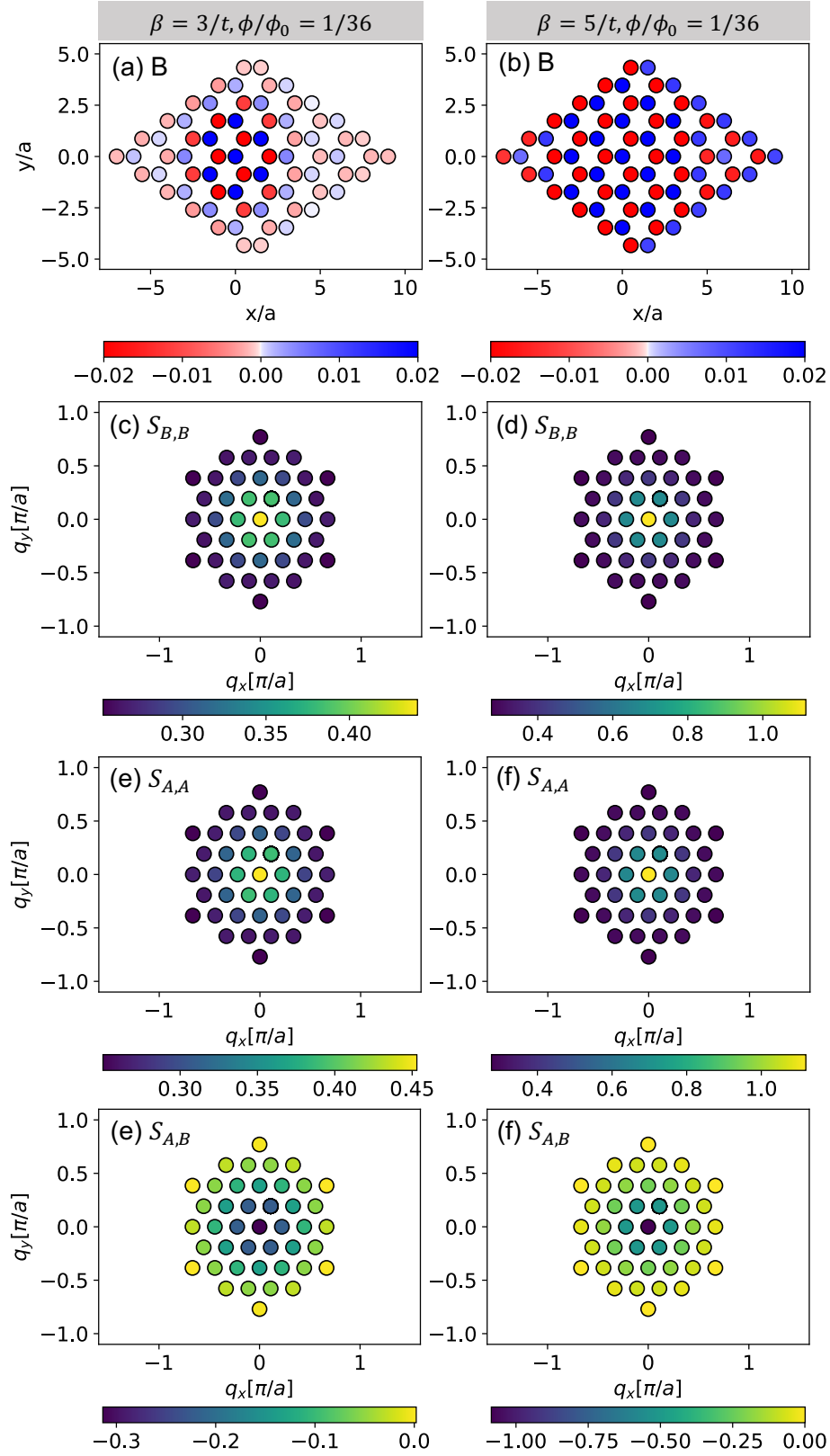


Figure 4. Zero-frequency spin susceptibility at half-filling for the topologically trivial case $t' = 0, M = 1$. The left and right columns show the susceptibility at the temperature $\beta = 3/t$ and $\beta = 5/t$ respectively. The first row displays $S_{m,B}(\mathbf{r}, \omega = 0)$ ($m = A, B$) in real space. The second, third rows show $S_{B,B}(\mathbf{q}, \omega = 0)$, $S_{A,A}(\mathbf{q}, \omega = 0)$ and $S_{A,B}(\mathbf{q}, \omega = 0)$ in momentum space, respectively. The interaction strength is $U/t = 12$ and the smallest magnetic flux of $\phi/\phi_0 = 1/36$ is applied for all panels.